Available online at www.sciencedirect.com
SCIENCE DIRECT
Polymer 47 (2006) 624–638
polymer
www.elsevier.com/locate/polymer

Elastomer particle morphology in ternary blends of maleated and non-maleated ethylene-based elastomers with polyamides: Role of elastomer phase miscibility

J.J. Huang, H. Keskkula, D.R. Paul *

Department of Chemical Engineering and Texas Materials Institute, The University of Texas at Austin, Austin, TX 78712, USA

Received 4 October 2005; received in revised form 30 November 2005; accepted 30 November 2005

Abstract

The elastomer particle morphology in ternary blends of maleated and non-maleated ethylene-based elastomers with polyamides has been examined. The elastomers used include an ethylene/propylene copolymer, EPR, with a maleic anhydride (MA) grafted version, EPR-*g*-MA, and an ethylene/1-octene copolymer, EOR, with maleated versions EOR-*g*-MA-*X*% where *X* is 0.35, 1.6 or 2.5. The polyamides used were nylon 6 and an amorphous polyamide, Zytel 330 from DuPont. The morphology development was explored from both thermodynamic and kinetic points of view where the former refers to miscibility of the elastomers and the latter might include the ratio of the elastomers, the matrix type, the order of mixing, mixing intensity, i.e. the extruder type, and graft structure, etc. Both sources influence the morphology developed. For ternary blends with EPR-*g*-MA/EPR, the morphology (particle size and distribution) seems to be well controlled via the level of maleation in the rubber phase. The two polyamides generate comparable rubber particle sizes at the same of MA level. For ternary blends with EOR-*g*-MA/EOR, the morphology strongly depends on the level of MA; the rubber particle size, in general, is much smaller in nylon 6 blends than in Zytel 330 blends. Morphology of ternary blends with EOR-*g*-MA/EOR is much more complex than that of blends with EPR-*g*-MA/EPR due to the co-existence of miscibility limits and the kinetic factors. Miscibility of maleated EOR elastomers is examined via transmission electron microscopy (TEM) using a special staining technique; a miscibility boundary, as revealed by TEM, occurs around $\Delta(\%MA) = 0.9 - 1.25$ MA%. If the two elastomers are miscible, a unimodal particle size distribution always appears in blends regardless of the kinetic factors; however, if immiscibility prevails, either a unimodal or bimodal particle size distribution may develop depending on the ratio of the elastomers and the matrix type. The order of mixing and the mixing intensity do not seem to change the modality of the size distribution.

Keywords: Miscibility; Amorphous polyamide; Morphology

1. Introduction

Toughening of semi-crystalline polyamides, like nylon 6 and 66, by blending with functionalized elastomers has been extensively reported [1–17]. Extensive efforts have been made to tailor the morphology of the dispersed elastomer phase, and it is well established that particle size and its distribution play a crucial role in governing the level of toughening [10,16,18]. Of course, other issues like the elastomer type and content are important as well. The focus of recent work [16,19,20] has been on the mechanistic reasons for why there are minimum and maximum elastomer particle sizes for generating super-tough blends.

An early proposal by Wu [4] suggested that the key parameter is interparticle distance rather than particle size per se. The majority of the literature [6,7,21–25] interprets the scale effects in terms of cavitation of the rubber phase and the subsequent triggering of shear yielding of the matrix due to relief of the state of triaxial tension ahead of the advancing crack. Another point of view is that rubber particles can alter the crystalline structure of the matrix in ways that facilitate toughening [15,26]. Recent work by Leibler et al. has addressed this issue through experiments that alter the crystalline organization of the matrix [27]. Certainly a better understanding of how the matrix morphology and characteristics affect toughening and other performance parameters is needed.

Our strategy has been a more extreme one in which we seek to compare the toughening responses and mechanisms of

* Corresponding author. Tel.: +1 512 471 5392; fax: +1 512 471 0542.
E-mail address: drp@che.utexas.edu (D.R. Paul).

0032-3861/$ - see front matter © 2005 Elsevier Ltd. All rights reserved.
doi:10.1016/j.polymer.2005.11.087

a purely amorphous polyamide (Zytel 330 from Du Pont) with that of the more well-investigated semi-crystalline polyamides like nylon 6, nylon 66, etc. In a prior paper [28], we demonstrated the toughening of this amorphous polyamide using combinations of a styrene-triblock copolymer having a hydrogenated mid-block, SEBS, with a maleic anhydride functionalized version, SEBS-*g*-MA, of this elastomer. In many ways the toughening behavior of this amorphous polyamide was rather similar to that of the semi-crystalline polyamides. In that work, it was possible to demonstrate that there is an upper limit on rubber particle size for effective toughening just as in the case of the crystalline polyamides. However, unlike the case of nylon 6, we were not able to generate small enough rubber particles to establish any lower size limit for this amorphous polyamide. This difficulty stems in part from the end-group configuration of this amorphous polyamide which makes it difficult to make the needed small particles. A maleated rubber capable of forming a wider range of rubber particle sizes including both the upper and the lower limit would be desirable for making this comparison of the toughening of amorphous versus crystalline polyamides. In addition, we were interested in exploring how the nature of the elastomer phase affects the toughening response of the two classes of polyamides.

Thus, we have extended our previous work to include maleic anhydride functionalized ethylene–propylene (EPR) and ethylene-1-octene (EOR) random copolymers for toughening. Our commercial sources of maleated EPR did not identify materials with grafting levels higher than 1.14 wt% MA. However, we were able to acquire a series of EOR elastomers with maleic anhydride grafting levels up to 2.5 wt%. These higher grafting levels provide more possibilities of generating smaller particle sizes. Interestingly, only a few reports have appeared on toughening polyamides using such maleated EOR elastomers [29,30].

The morphology (particle size and its distribution) of the dispersed phase may be controlled via the level of maleation in the rubber phase by using a mixture of maleated and non-maleated elastomers in varying proportions in the formulation. Such use of a combination of maleated and non-maleated elastomers has been reported to be a simple but effective way for tailoring rubber particle size [10,14,17], although doing so may potentially incur immiscibility between the two elastomer components due to the increased polarity caused by maleation. That is, two maleated rubbers with different levels of MA may not necessarily be miscible depending on the difference in MA level and their molecular weights. Such immiscibility, if it exists, complicates the morphology development during reactive blending with polyamides and may lead to bimodality in rubber particle distribution as has been reported in ternary blends of nylon 6 with maleated and non-maleated polypropylene [31]. Thus, it is useful to know if these maleated elastomers with different levels of MA are miscible with each other or not. In addition to the thermodynamics effects (miscibility), many kinetic or non-equilibrium factors influence the morphology of a blend; some of these factors might include: the ratio of two elastomers, the matrix type, the order of mixing, mixing intensity, i.e. the extruder type, and graft structure, etc. Obviously, the co-existence of both thermodynamic and kinetic factors makes the morphology development even more complicated. The morphology, undoubtedly, determines the final mechanical properties including Izod impact strength of the blend.

The broader purpose of this work is to explore and compare in some detail the toughening effect between a semi-crystalline (nylon 6) and an amorphous polyamide matrix (Zytel 330) using combinations of EPR with a maleated version, EPR-*g*-MA, and, combinations of EOR with maleated versions, EOR-*g*-MA-*X*%. This paper reports the effects of miscibility, as revealed by transmission electron microscopy (TEM), between maleated EOR elastomers with different levels of MA, i.e. EOR-*g*-MA-*X*% versus EOR-*g*-MA-*Y*% ($X \neq Y$), on the nature of the rubber particle size distribution in blends with both polyamides. In addition, the effects of kinetic factors including the ratio of two elastomers, the matrix type, the order of mixing and mixing intensity, i.e. the effect of extruder type on the morphology development of blends will be presented. A subsequent paper [32] will report rubber toughening effects of these two types of rubbers when nylon 6 and Zytel 330 are the matrix polymers. The effects of rubber content, rubber particle size and its distribution associated with these thermodynamic and kinetic factors on Izod impact strength and the ductile–brittle transition temperature will be considered. A final paper [33] will explore the fracture behavior of selected blends in more detailed ways.

2. Experimental section

Table 1 summarizes pertinent information about the materials used in this study. The structure of the amorphous polyamide [28,34] has been described previously. The EPR and EPR-*g*-MA have been used in prior work from this laboratory for toughening semi-crystalline polyamides [10,17]. The ethylene-1-octene copolymer, designated as EOR, is the precursor material for maleated versions [35], designated as EOR-*g*-MA-*X*%, where *X* is 0, 0.35, 1.6 or 2.5. Prior to melt compounding, all materials containing nylon 6 and a-PA were pre-dried for at least 16 h in a vacuum oven at 80 °C while the elastomers were dried for at least 16 h in a convection oven at 65 °C. Most blends containing nylon 6 and all blends containing a-PA were prepared using a Haake co-rotating, intermeshing twin screw extruder ($D = 3.05$ cm, $L/D = 10$) operated at 240 °C and 280 rpm; the configuration of mixing elements in this extruder was described previously [28]. Selected blends containing nylon 6 were prepared using a Killion single screw extruder ($D = 2.54$ cm, $L/D = 30$) having an intensive mixing head operated at 240 °C and 40 rpm. Binary blends of the EOR elastomers (without polyamides), used for examination of miscibility, were made in the single screw extruder at the same processing conditions.

The effect of the order of mixing of the three components on blend morphology was explored using three different sequences of adding the various components. Most of the blends were made by vigorously mixing all components

Table 1
Materials used

Designation used here	Materials (commercial designation)	Composition/specification	Molecular weight	Brabender torque (N m)[a]	Supplier
a-PA[b]	Zytel 330	$[COOH]/[NH_2]=4.5$[c] $T_g=127$ °C	$\bar{M}_n=14000$[d] $\bar{M}_w=50000$[d]	10.7	Du Pont
Nylon 6[e]	B73WP[f]	$[COOH]/[NH_2]=0.9$	$\bar{M}_n=22000$	6.37[g]	Honeywell (formerly Allied-Signal)
EOR	Exact 8201	28 wt% Octene; MFR: ~22 g/10 min[h]; density=0.884 g/cc[i]	$\bar{M}_n=52000$[i] $\bar{M}_w=116000$[i] $\bar{M}_z=211000$[i]	9.5	ExxonMobil
EOR-*g*-MA-0.35%	Exxelor VA 1840	28 wt% Octene; 0. 35 wt% MA; MFR: ~25 g/10 min[h]; density=0.8865 g/cc[i]	$\bar{M}_n=46000$[i] $\bar{M}_w=121000$[i] $\bar{M}_z=254000$[i]	9.2	ExxonMobil
EOR-*g*-MA-1.6%	Exxelor MDEX 101-2	28 wt% Octene; 1.6 wt% MA; MFR: 19 g/10 min[h]; density=0.8913 g/cc[f]	$\bar{M}_n=29000$[i] $\bar{M}_w=134000$[i] $\bar{M}_z=417000$[i]	6.9	ExxonMobil
EOR-*g*-MA-2.5%	Exxelor MDEX 101-3	28 wt% Octene; 2.5 wt% MA; MFR: 20 g/10 min[h]; density=0.8960 g/cc[i]	$\bar{M}_n=16000$[i] $\bar{M}_w=103000$[i] $\bar{M}_z=268000$[i]	6.3	ExxonMobil
EPR	Vistalon 457	53 wt% propylene	$\bar{M}_w=54000$ $\bar{M}_w/\bar{M}_n=2$	14.2[g]	ExxonMobil
EPR-*g*-MA	Exxelor 1803	53 wt% propylene 1.14 wt% MA	$\bar{M}_n=40000-50000$	9.76[g]	ExxonMobil

[a] Measured after 10 min at 240 °C and 60 rpm.

[b]
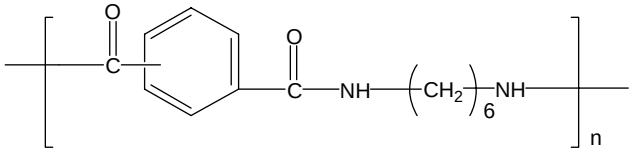

[c] Data from Ref. [38].
[d] Data from Ref. [34].
[e] Referred to as MMW nylon 6 in Ref. [28].
[f] Formerly Capron 8207F.
[g] Data from Ref. [17].
[h] Data at 230 °C and 10 kg and provided by the supplier.
[i] Measured by ExxonMobil at Baytown, TX, USA.

together prior to feeding simultaneously into the extruder, i.e. only one extrusion pass. For selected blends of nylon 6 with EOR/EOR-*g*-MA-*X*%, the two rubber components were premixed in the desired proportions in either a twin screw or a single screw extruder in a first extrusion pass. The premixed rubber material was then melt blended with nylon 6 in either the twin screw or the single extruder in a second extrusion pass. Likewise, for selected blends of a-PA with EOR/EOR-*g*-MA-*X*%, the premixing and subsequent melt blending were carried out only in the twin screw extruder. For selected blends of nylon 6 with EOR/EOR-*g*-MA-*X*%, a master batch of 50 wt% EOR and 50 wt% nylon 6 was formulated in either the twin screw or the single screw extruder in a first extrusion pass; the master batch material was then melt blended with additional nylon 6 and EOR-*g*-MA-*X*% in either the twin screw or the single screw extruder in a second extrusion pass. Likewise, for selected blends of a-PA with EOR/EOR-*g*-MA, formation of a similar master batch and subsequent melt blending with additional a-PA and EOR-*g*-MA were made only in the twin screw extruder. For blends containing EPR/EPR-*g*-MA, owing to the bale form of the as-received EPR, a master batch of 50 wt% EPR and 50 wt% a-PA was prepared in a 250 ml Brabender Plasticorder at 240 °C and 60 rpm; the master batch was then melt blended with additional a-PA and EPR-*g*-MA in the twin screw extruder. These procedures have been described more fully elsewhere [17].

The extruded blends were pelletized and then molded into standard tensile (ASTM D638, Type I) and Izod (ASTM D256) bars using an Arburg Allrounder 305-210-700 injection molding machine under the following conditions: a barrel temperature of 240 °C (250 °C for the nozzle), a mold temperature of 80 °C, an injection molding pressure of 70 bars, a holding pressure of 35 bars and 150 rpm of the screw.

Blend morphology was determined by TEM using ultra-thin sections cryogenically microtomed from the far end of a Izod bar that were cut from the plane perpendicular to the flow direction unless specified otherwise. The thin sections (25 nm thick) were obtained using a Reichert-Jung Ultracut E microtome equipped with a diamond knife operated at −40 °C. The polyamide phase was stained for an hour with a

2 wt% aqueous solution of phosphotungstic acid (PTA). Two transmission electron microscopes were used to view the thin sections: a JOEL 200CX operating at 120 kV or a JOEL 2010F operating at 120 or 200 kV. A semi-automated digital analysis technique was employed to calculate the rubber particle size from the TEM photomicrographs using NIH Image® software. No attempt was made to convert the apparent particle diameter into a true particle size [17] since such corrections are very difficult to do properly when there is a distribution of sizes as recently demonstrated by Corte and Leibler [36]. It is believed that use of apparent sizes does not alter our conclusions; in any case, the prior literature is based on uncorrected sizes. Typically, at least 800 particles from different views from two different Izod bars (in most blends) were analyzed. For blends with large particles, at least 200 particles were collected for analysis. For blends exhibiting bimodality in morphology, an average particle diameter was computed for each of the two populations (e.g. see values in subsequent tables for ternary blends) as well as the global average over both populations. Number, weight and volume average rubber particle sizes were calculated from the distribution of sizes using the following equations

$$\bar{d}_{\mathrm{n}} = \frac{\sum n_i d_i}{\sum n_i}$$

$$\bar{d}_{\mathrm{w}} = \frac{\sum n_i d_i^2}{\sum n_i d_i}$$

$$\bar{d}_{\mathrm{v}} = \frac{\sum n_i d_i^4}{\sum n_i d_i^3}$$

a more detailed discussion on particle size measurement and calculation is available elsewhere [28]. In this work, representation of rubber particle size analysis becomes a critical issue particularly when bimodality in morphology exists for a blend. A detailed discussion on graphic representation of particle size analysis will be given in a later section.

An essential part of this work deals with whether any two EOR elastomers with different levels of maleation, including zero, are miscible or not. Examination of the morphology via TEM in these binary rubbery blends is problematic due to the lack of phase contrast stemming from the chemical similarity of the two components and the fact that staining agents, used to induce phase contrast, react similarly with both phases. However, this problem was solved by a special staining technique [37] used previously in this laboratory for examining the miscibility of PP/PP-*g*-MA blends [31]. This technique involves first reacting the grafted maleic anhydride groups with *m*-xylene diamine to introduce aromatic, amide, and amine groups into the EOR-*g*-MA phase that are capable of being stained by RuO_4. In this way, the necessary phase contrast is created for TEM examination. The reaction occurred by exposing the mesa-cut of elastomer blends to the vapor of the diamine at 75 °C for 2–4 h in a vial (1.66 cm of outer diameter and 6.22 cm high) with a cap in a silicon oil bath. The mesa-cut was obtained by trimming a block of an Izod bar previously glued onto a mounting cylinder into a dimension of about $0.2 \times 0.2\ \mathrm{mm}^2$ (the final size for microtoming) with a glass knife at −100 °C using a RMC PowerTome Ultramicrotome XL. The mounting cylinder with the mesa-cut was then glued onto the cap of the vial while keeping the mesa-cut face down for reaction. After the reaction, the mesa-cut was pre-stained with RuO_4 in another vial for 10 min. The pre-stained mesa-cut was microtomed for obtaining ultra-thin (25 nm) sections for TEM examination at −100 °C using either of the two microtomes described above. The collected ultra-thin sections were then stained with RuO_4 for 20 min. The miscibility was examined on these stained ultra-thin sections using a JOEL 2010F transmission electron microscope operating at 200 kV and under scanning transmission electron microscope (STEM) mode.

3. Graphic representation of particle size analysis

In this work, the rubber particle distribution is represented purposely as 'area of particles/unit area' as a function of 'apparent particle diameter'. Such a representation is important and powerful for demonstrating bimodality, if it exists, of particle sizes. Other representations, e.g. frequency versus apparent particle size, in our experience do not always capture the characteristic of bimodality even though this may be clearly evident to the eye. To illustrate this with an extreme example, suppose that the image shows 500 rubber particles of which 495 are of size 0.1 μm, two particles are of size 0.8 μm, and three particles are of size 1 μm. In terms of area, the five particles of size 0.8 and 1 μm correspond to 428 particles with a size of 0.1 μm; clearly these larger particles cannot be ignored even though in terms of frequency they represent only 1% of the particles present. We have found that 'area of particles/unit area' versus 'apparent particle diameter' is more reasonable for presenting the true features of such a distribution. In addition, careful attention must be paid to how the distribution plot is created from the digital file of a finite number of particles each with a given size. It is necessary to group the particles within a certain size range to make this plot. Selection of this step or bin size is critical for revealing bimodality. If the step size is too small, the distribution curve may not be smooth and the trend may not be well defined or a false bimodality may appear. On the contrary, if the step size is too large, the bimodality may not be seen, although the distribution curve is smooth. For log-normal type distributions, we have found that a linear step size is inappropriate. When a linear step size is used, a bin size that is appropriate for the small particles will be much too small for the larger particles and vice versa. A logarithmic step size has been used in our work to solve this problem. Typically, we have found that dividing the size scale into bins where the next incremental range is 1.2–1.4 times larger than the last one works well. The particle size associated with the peak(s) of a distribution is rather close to the weight average rubber particle size value.

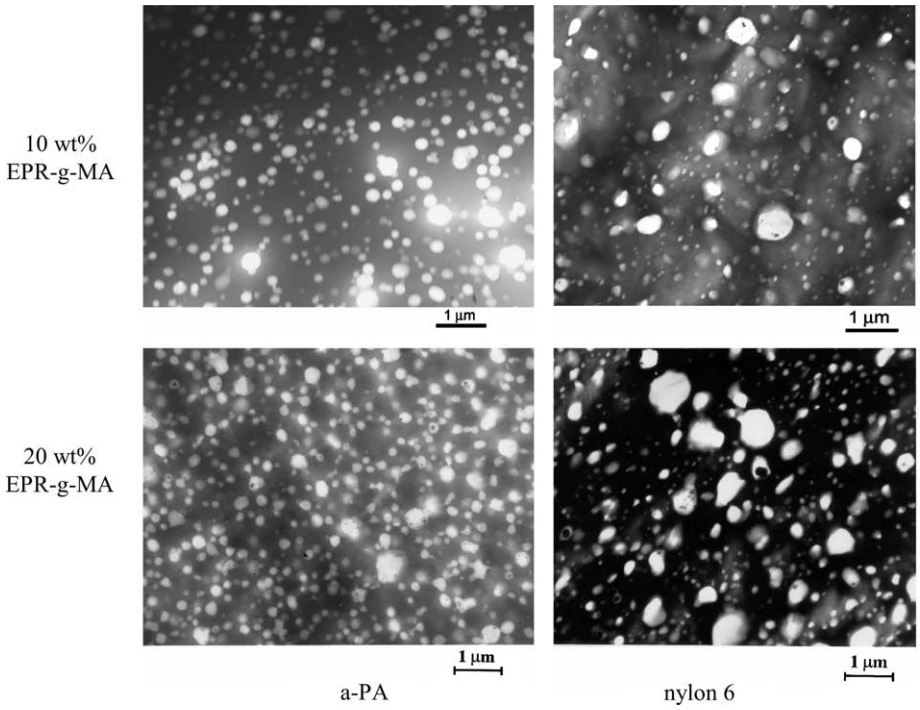

Fig. 1. TEM photomicrographs of binary blends of EPR-*g*-MA with a-PA and with nylon 6 containing 10 and 20 wt% EPR-*g*-MA. The polyamide phase is stained dark with phosphotungstic acid.

4. Morphology of binary blends of a-PA and nylon 6 with a maleated rubber

4.1. EPR-g-MA

Fig. 1 compares the morphology of binary blends based on a-PA with those based on nylon 6 containing 10 and 20 wt% EPR-*g*-MA. Rubber particles in all blends appear fairly regular and quite round in shape; the blends of a-PA seem to exhibit more uniform dispersion of rubber particles than do those of nylon 6. Table 2 summarizes the rubber particle sizes and polydispersities of the blends examined. For a-PA, the rubber particle size, in general, increases slightly with EPR-*g*-MA content, as might be expected, due to higher probability of coalescence of rubber particles. For nylon 6, however, the trend is more complex and may reflect a variety of issues beyond the scope of this work as shown in the previous study of SEBS-*g*-MA/a-PA blends [28] made in the same single screw extruder. The a-PA blends are seen to be less polydisperse than those of corresponding nylon 6 blends.

4.2. EOR-g-MA-X%

Fig. 2 shows how the morphology of binary blends of the two polyamides with the EOR-*g*-MA-*X%* elastomers described earlier depends on the maleic anhydride level. As can be seen, without MA, the rubber particles are very large and do not adhere well to the matrix; as a small amount of MA, i.e. 0.35%, is added, the rubber particle size is reduced dramatically especially for nylon 6. The rubber particles sizes are reduced even further with higher MA levels. Fig. 3 shows the rubber particle size distribution for the binary blends shown in Fig. 2. There is a log-normal type of distribution of rubber particle sizes for each MA level in each of the two polyamides which shifts to smaller sizes with higher MA levels. The particle size distribution for nylon 6 blends is narrower and shifts relatively more towards smaller sizes than seen for a-PA blends. For both matrices, the decrease in particle size is relatively small as the MA level increases from 1.6 to 2.5 wt%. Table 3 summarizes the rubber particle size analysis for the binary blends. For both polyamides, the weight average rubber particle size decreases significantly with MA; however, it decreases much more for nylon 6 blends than for a-PA blends; over this range of maleic anhydride contents, the weight average rubber particle size decreases by nearly two orders of magnitude for nylon 6 blends but only a little more than one order of magnitude for a-PA

Table 2
Summary of rubber particle size for binary blends of a-PA or nylon 6 with EPR-*g*-MA

Matrix	wt % rubber	Extruder type	$\bar{d}_w$ (μm)	$\bar{d}_w/\bar{d}_n$	$\bar{d}_v/\bar{d}_n$
a-PA	5	Twin	0.14	1.22	1.73
	7.5	Twin	0.17	1.14	1.51
	10	Twin	0.18	1.15	1.54
	12.5	Twin	0.16	1.11	1.39
	15	Twin	0.19	1.17	1.68
	20	Twin	0.20	1.18	1.70
Nylon 6	5	Single	0.29	1.85	5.2
	10	Single	0.16	1.32	2.06
	15	Single	0.18	1.47	3.27
	20	Single	0.20	1.42	2.72

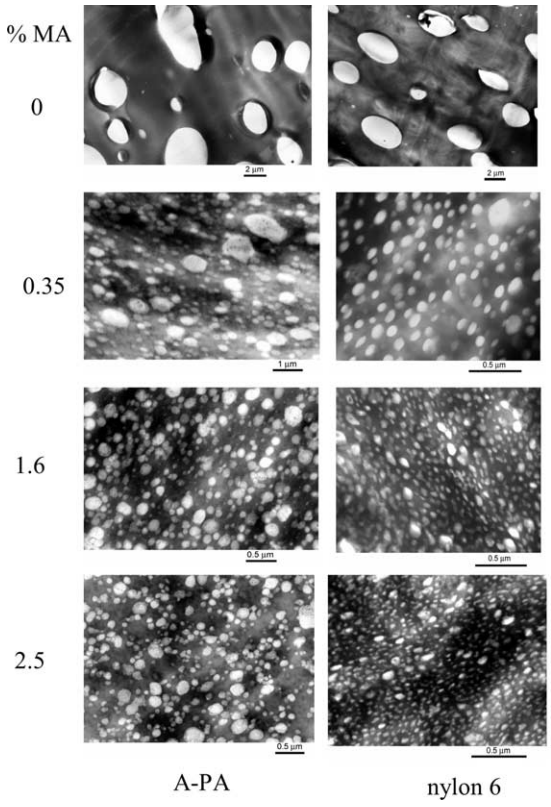

Fig. 2. TEM photomicrographs of binary blends of 20:80 EOR-*g*-MA-*X*% (*X*= 0, 0.35, 1.6, 2.5)/polyamide where the matrix is a-PA or nylon 6. The polyamide phase is stained dark with phosphotungstic acid.

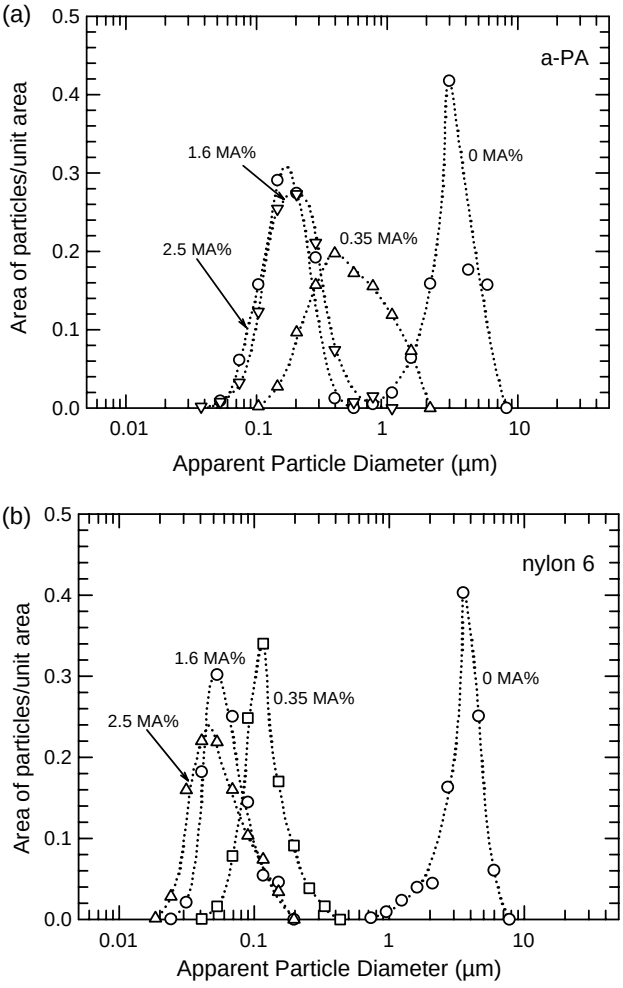

Fig. 3. Rubber particle size distributions for the binary blends of EOR-*g*-MA-*X*% with a-PA (a) and with nylon 6 (b) shown in Fig. 2.

blends. Also, the nylon 6 blends, in general, show a lower polydispersity. Although this difference in rubber particle size between a-PA and nylon 6 blends may be somewhat a result of rheological effects, i.e. the viscosity of nylon 6 is more closely matched to that of the EOR-*g*-MA material than is the case for a-PA, the molecular difference between these two polyamides plays a more important role. It is well-known that maleated rubber particles formed in nylon 66 are larger and more complex in shape than those formed in nylon 6 [11]. This is a result of the fact that a certain fraction of nylon 66 chains have two amine groups that can lead to cross-linking type effects; whereas, typically all the nylon 6 chains have only one amine end. Since a-PA is made from diamine and dibasic acid monomers, its end group configuration should be more like nylon 66 than nylon 6. However, the particle size and shapes in a-PA are not as different from those in nylon 6 as would be expected for nylon 66. The chains of a-PA have been reported to be rich in [COOH] groups [38], i.e. $[COOH]/[NH_2]=4.5$ as shown in Table 1. This is somewhat unusual, since typical polyamides such as nylon 6 or nylon 66 have balanced [COOH] and $[NH_2]$ groups, i.e. $[COOH]/[NH_2]\approx 1$, unless the polyamide is made to be rich in one or the other end-groups for some particular purpose. The lower content of amine groups for reacting with MA groups of EOR-*g*-MA potentially reduces the number of graft chains formed by reaction with maleic anhydride and appears to moderate the incidence, or at least the consequence, of two amines per chain. This speculation is corroborated by the fact that nylon 6 blends always consume more power during extrusion at the same composition and feeding rate.

The shape of the rubber particles observed here for a-PA blends does not exhibit the complex morphology where rubber particles are very large, irregular with considerable occlusions like that seen in nylon 66 and other nylon *x*, *y* type matrices attributed to the 'cross-linking' type effects that originate from existence of some fraction of chains having two amine end-

Table 3
Rubber particle size dependence on %MA in the rubber phase for binary blends containing EOR-*g*-MA-*X*%

Matrix	%MA in rubber	$\bar{d}_w$ (μm)	$\bar{d}_w/\bar{d}_n$	$\bar{d}_v/\bar{d}_n$
a-PA	0	2.41	1.26	1.78
	0.35	0.35	1.39	2.83
	1.6	0.14	1.26	1.96
	2.5	0.13	1.20	1.64
Nylon 6	0	2.70	1.37	1.72
	0.35	0.097	1.10	1.44
	1.6	0.051	1.10	1.40
	2.5	0.043	1.16	1.73

groups. The high ratio of [COOH]/[NH_2] of a-PA may, statistically, lead to relatively smaller fraction of chains having two amine end-groups than is typical of nylon *x*, *y* materials. The extent of such reactions that may occur would explain the broader distribution of sizes seen in a-PA and the fact that the particles are as small as those seen in nylon 6 at a given maleic anhydride content.

5. Morphology of ternary blends of a-PA and nylon 6 with combinations of rubbers

5.1. EPR-g-MA/EPR

Fig. 4 shows the rubber particle distribution and morphology of ternary blends of a-PA containing 20 wt% of an EPR-*g*-MA/EPR mixture with proportions of 20:80 and 60:40. The distributions are of the log-normal type, and the particles shifts to smaller sizes with a higher fraction of EPR-*g*-MA. Fig. 5 compares the weight average rubber particle size as a function of the MA level of the rubber phase, calculated from the MA content of the two elastomer components and their

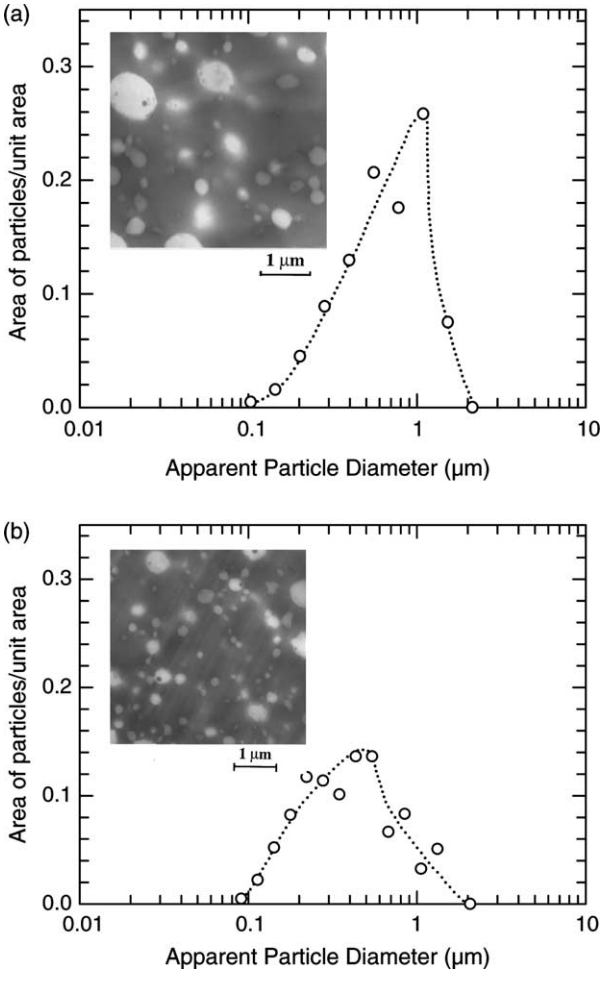

Fig. 4. TEM photomicrographs and rubber particle size distribution for ternary blends of a-PA with EPR-*g*-MA/EPR mixtures (rubber phase is 20% by weight of the total blend) in proportions of 20:80 (a) and 60:40 (b). The polyamide phase is stained dark with phosphotungstic acid.

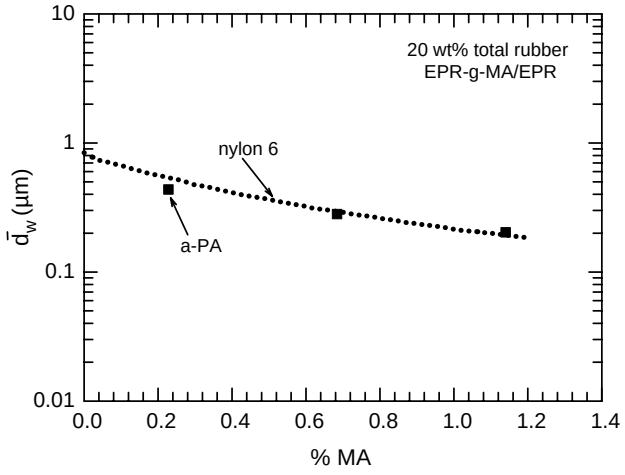

Fig. 5. Comparison of rubber particle size for ternary blends of EPR-*g*-MA/EPR mixtures (rubber phase is 20% by weight of the total blend) in a matrix of a-PA and in a matrix of nylon 6 as a function of the MA level in the rubber phase.

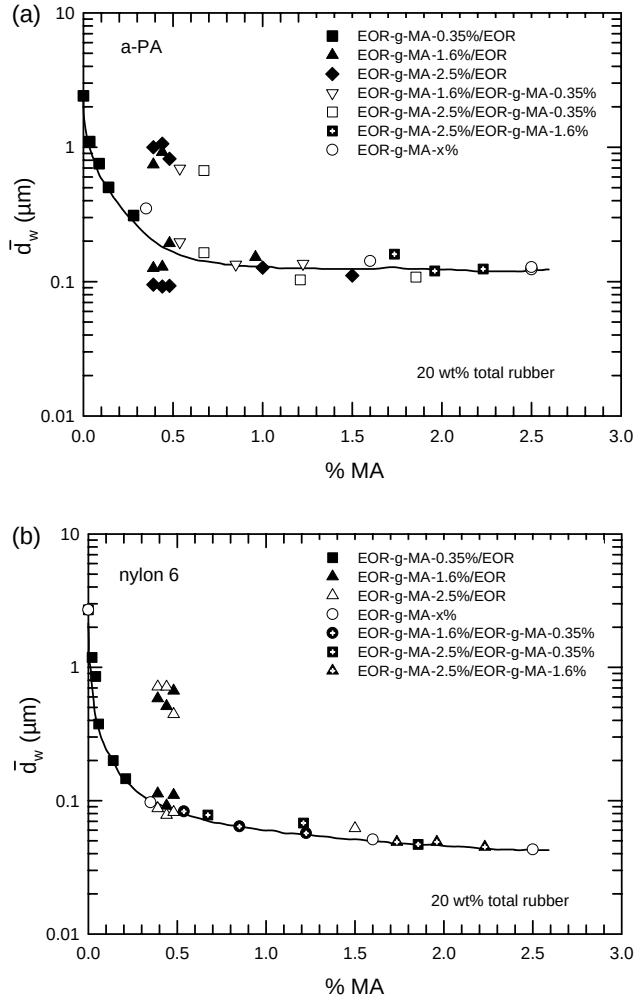

Fig. 6. Effect of the MA level in the rubber phase on the rubber particle size for ternary blends with 20 wt% total rubber comprised of various combinations of the four EOR elastomers in a matrix of a-PA (a) and in a matrix of nylon 6 (b).

proportions in the rubber phase, for a-PA and nylon 6 ternary blends. The rubber particle size decreases gradually with the MA level. The two polyamides generate comparable rubber particle sizes at the same MA level.

5.2. EOR-g-MA/EOR or EOR-g-MA-X%/EOR-g-MA-Y% (X≠Y)

5.2.1. Effect of maleic anhydride level in the rubber phase on morphology development

As seen in Fig. 5, the smallest particle size that can be generated using the EPR-*g*-MA elastomer system is about 0.2 μm in both polyamides which is not small enough to fully define the lower size limit for toughening. However, the series of maleated EOR elastomers is capable of generating smaller rubber particles as shown in Table 3, particularly for nylon 6 because of the higher levels of maleation available. Thus, as can be visualized, a wider range of elastomer particle sizes may be generated by using mixtures of two maleated EOR elastomers with different MA levels in varying proportions. Fig. 6 shows the rubber particle size as a function of MA level in the rubber phase for blends of both polyamides based on all six combinations of the four EOR-based elastomers in various proportions while maintaining the total rubber phase content at 20 wt%. For a-PA, the rubber particle size is reduced considerably as the MA level is increased to 0.7 wt% where it seems to plateau. Bimodality of rubber particle size was observed for some blends based on mixtures of EOR or EOR-*g*-MA-0.35% with EOR-*g*-MA-1.6% or EOR-*g*-MA-2.5%. In Fig. 6, bimodality is indicated by plotting the average size of each of the two populations at the indicated rubber phase MA level. Interestingly, bimodality seems to be observed only over some range of proportions between the two elastomer components for the pairs mentioned. Similarly, the rubber particle size depends strongly on the calculated MA level in the rubber phase for nylon 6 blends; the rubber particle size decreases dramatically with MA content up to about 0.6 wt% but more gradually beyond this level. Again, bimodality is observed but this seems to occur only for blends based on mixtures of EOR with EOR-*g*-MA-1.6% and EOR-*g*-MA-2.5% and for certain proportions between the components. An example of the bimodality shown in Fig. 6 is given in Fig. 7 where the rubber phase consists of EOR-*g*-MA-2.5%/EOR mixtures in proportions of 16:84 and 60:40 for both polyamides. Clearly, a bimodal particle size distribution is seen, regardless of the matrix type, when the proportion is 16:84; the two populations differ by about an order of magnitude in size. However, a unimodal distribution is seen

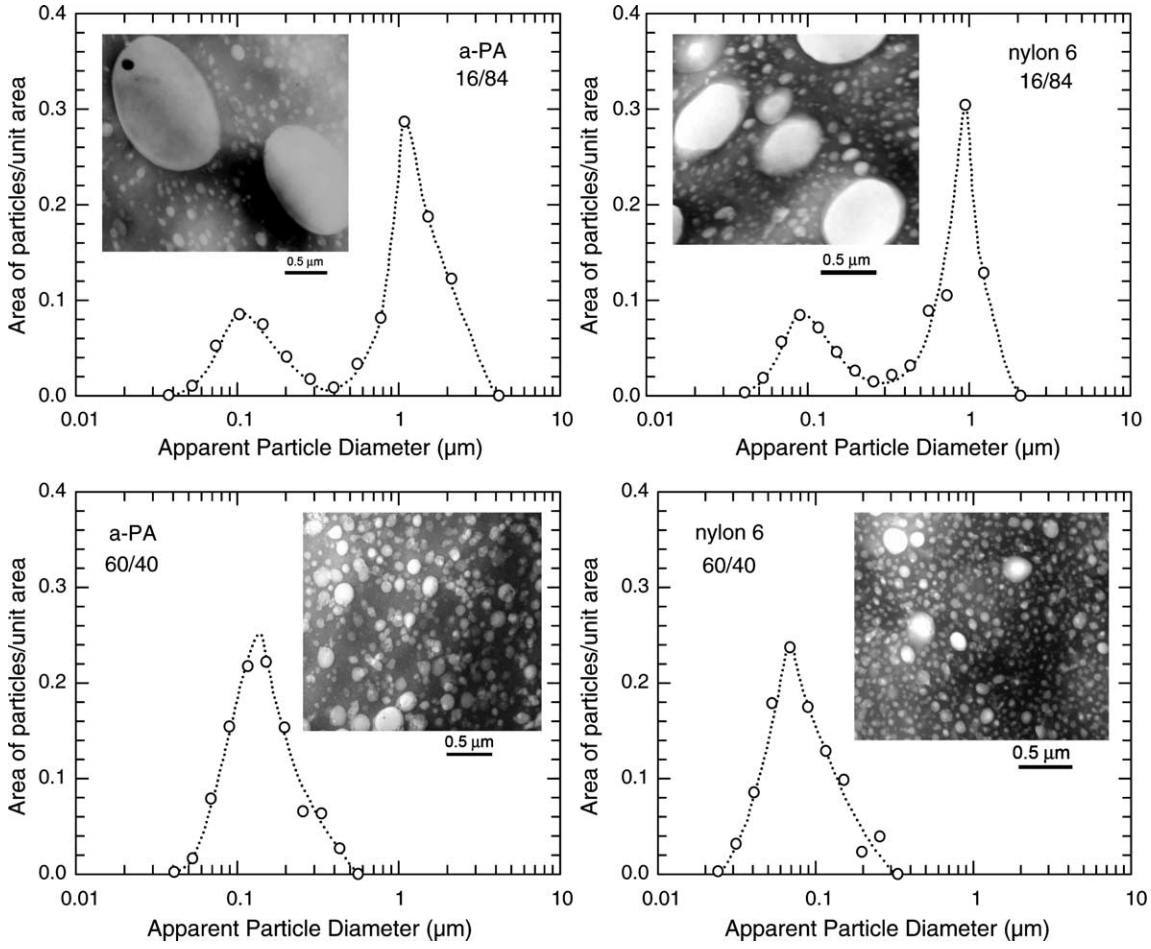

Fig. 7. TEM photomicrographs and rubber particle size distributions for ternary blends containing a total 20 wt% of the rubber phase comprised of mixtures of EOR-*g*-MA-2.5% with EOR in a proportion of 16:84 and 60:40 where the matrix is a-PA or nylon 6. The polyamide phase is stained dark with phosphotungstic acid.

for both polyamides when the two elastomers are mixed in the proportion of 60:40. The bimodality of rubber particle sizes apparently reflects several issues that affect morphology development. We hypothesize that both thermodynamic and kinetic factors are at play. The thermodynamic issue refers to the state of miscibility between the two elastomers and the kinetic issue may be reflected in the ratio of two elastomers, the matrix type, the order of mixing, mixing intensity, i.e. the extruder type, and graft structure, etc. The following subsections will explore in some detail the causes of bimodality from these points of view.

5.2.2. Miscibility of the EOR elastomers with each other

Immiscibility of two EOR-based polymers could result from differences in their 1-octene content or the increased polarity caused by maleation. Since the non-maleated EOR used here is the precursor for the maleated ones, i.e. the same ethylene/1-octene ratio is maintained; thus, any immiscibility must result from the maleation difference. The state of miscibility of two polymers can be understood in terms of the Flory–Huggins theory [39]; the Gibbs free energy of mixing two dissimilar polymers, A and B, per unit volume of mixtures can be expressed as

$$\Delta g_{\mathrm{mix}} = RT\left(\frac{\rho_{\mathrm{A}}\phi_{\mathrm{A}}}{M_{\mathrm{A}}}\ln\phi_{\mathrm{A}} + \frac{\rho_{\mathrm{B}}\phi_{\mathrm{B}}}{M_{\mathrm{B}}}\ln\phi_{\mathrm{B}}\right) + B\phi_{\mathrm{A}}\phi_{\mathrm{B}} \qquad (1)$$

where ϕ_i is the volume fraction, is the mass density, is the molecular weight of component i, and B is the binary interaction density. The condition for stability in miscible blends is given by

$$\left(\frac{\partial^2 \Delta g_{\mathrm{mix}}}{\partial \phi_i^2}\right)_{\mathrm{T,P}} > 0 \qquad (2)$$

A miscible mixture is assured when B is less than a critical value, B_{c}, given by

$$B_{\mathrm{c}} = \frac{RT_{\mathrm{c}}}{2}\left[\sqrt{\frac{\rho_{\mathrm{A}}}{M_{\mathrm{A}}}} + \sqrt{\frac{\rho_{\mathrm{B}}}{M_{\mathrm{B}}}}\right]^2 \qquad (3)$$

The weight average molecular weight ($\bar{M}_{\mathrm{w}}$) [40–42] should be used in the evaluations for polydisperse polymers.

The binary interaction model [43–45] for blends of copolymers can be used to estimate the interaction energy density for the blends of non-maleated EOR and the maleaded version, EOR-*g*-MA, by considering EOR-*g*-MA as a random copolymer of EOR and maleic anhydride units. Based on this model, the net interaction energy density of mixing a random copolymer, A, composed of monomer units 1 and 2, with a

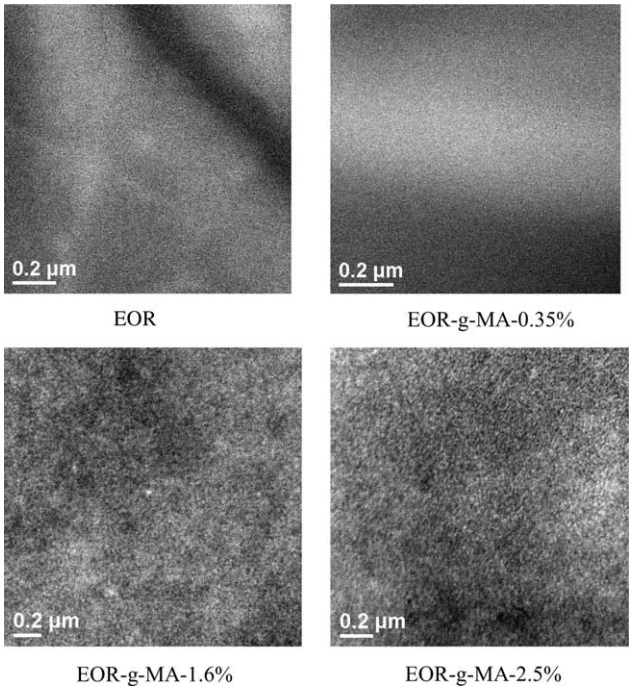

Fig. 8. TEM photomicrographs, using the STEM (dark field) mode, of the four neat EOR-based elastomers after staining and sectioning.

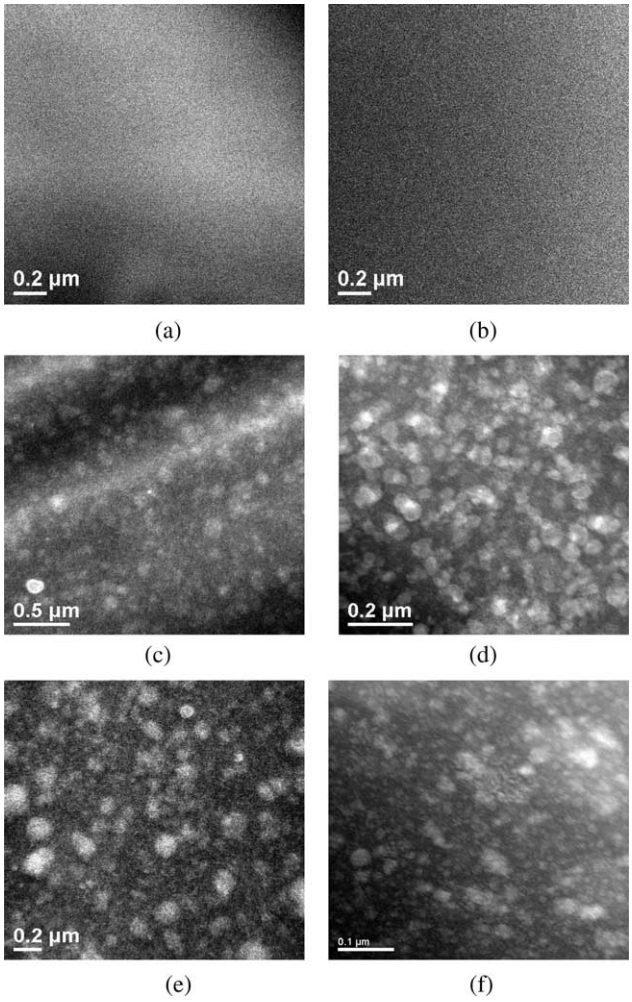

Fig. 9. TEM photomicrographs, using the STEM (dark field) mode, for six stained binary elastomer blends: (a) Δ(%MA)=0.35−0=0.35% (EOR-*g*-MA-0.35%/EOR); (b) Δ(%MA)=2.5−1.6=0.9% (EOR-*g*-MA-2.5%/EOR-*g*-MA-1.6%); (c) Δ(%MA)=1.6−0.35=1.25% (EOR-*g*-MA-1.6%/EOR-*g*-MA-0.35%); (d) Δ(%MA)=1.6−0=1.6% (EOR-*g*-MA-1.6%/EOR); (e) Δ(%MA)=2.5−0.35=2.15% (EOR-*g*-MA-2.5%/EOR-*g*-MA-0.35%) and (f) Δ(%MA)=2.5−0=2.5% (EOR-*g*-MA-2.5%/EOR).

homopolymer (the non-maleated EOR elastomer is treated as a homopolymer here), B, composed of monomer unit 1, is given by

$$B = B_{12}\left(\phi_2' - \phi_2''\right)^2 \quad (4)$$

where ϕ_2' is the volume fraction of maleic anhydride in one EOR-g-MA and ϕ_2'' is the volume fraction in the other; B_{12} is the interaction energy between EOR and maleic anhydride units. By combining Eqs. (3) and (4), one sees that there is a critical difference in maleic anhydride content, i.e. $\phi' - \phi_2''$ (or an equivalent difference in weight fraction), that defines the boundary between miscibility and immiscibility provided the molecular weight of the components are nearly the same. This critical difference in maleic anhydride content could be calculated if B_{12} were known. While solubility parameter theory provides one possibility to estimate B_{12}, the errors in estimating the solubility parameters are rather significant [31]. Rather than pursuing any scheme for predicting the critical difference in maleic anhydride content, Δ(%MA), that defines miscible combinations from immiscible ones, we will determine this experimentally via electron microscopy using the special staining technique described earlier.

Fig. 8 shows TEM images of the four neat EOR-based elastomers described in Table 1 after staining and sectioning as described earlier. These images show no significant features except some non-uniformity of intensity due to the variation in section thickness. Examination of each neat EOR elastomer in this way is necessary to serve as a control for the subsequent examination of such images for mixtures of two EOR-based elastomers. Furthermore, some commercial maleated products are blends and may be phase separated. Maleation of polypropylene generally results in severe molecular weight loss and to compensate for this some commercial products consist of mixtures of PP and PP-g-MA. The images in Fig. 8 establish that these EOR materials are not blends or, at least, are not phase separated mixtures of EOR-based components with different levels of MA.

Fig. 9 shows images of the six possible binary blends of the four EOR-based elastomers, after staining and sectioning, viewed in an STEM dark field mode. The combinations of EOR-g-MA-0.35%/EOR (Δ%MA = 0.35%) and EOR-g-MA-2.5%/EOR-g-MA-1.6% (Δ%MA = 0.9%) do not show phase separation and can be presumed to be miscible. However, the other four combinations, EOR-g-MA-1.6%/EOR-g-MA-0.35% (Δ%MA = 1.25%), EOR-g-MA-1.6%/EOR (Δ%MA = 1.6%), EOR-g-MA-2.5%/EOR-g-MA-0.35% (Δ%MA = 2.15%) and EOR-g-MA-2.5%/EOR (Δ%MA = 2.5%), show phase separation, indicating that the fours pairs are not miscible. Thus, the miscibility boundary occurs around Δ(%MA) = 0.9 − 1.25%. The STEM technique was employed to examine miscibility in this work rather than traditional TEM since the contrast between the phases even after this special staining technique is quite low. STEM, in some circumstances, is more advantageous than traditional TEM for improving phase contrast as a result of collecting signals from most of the scattered

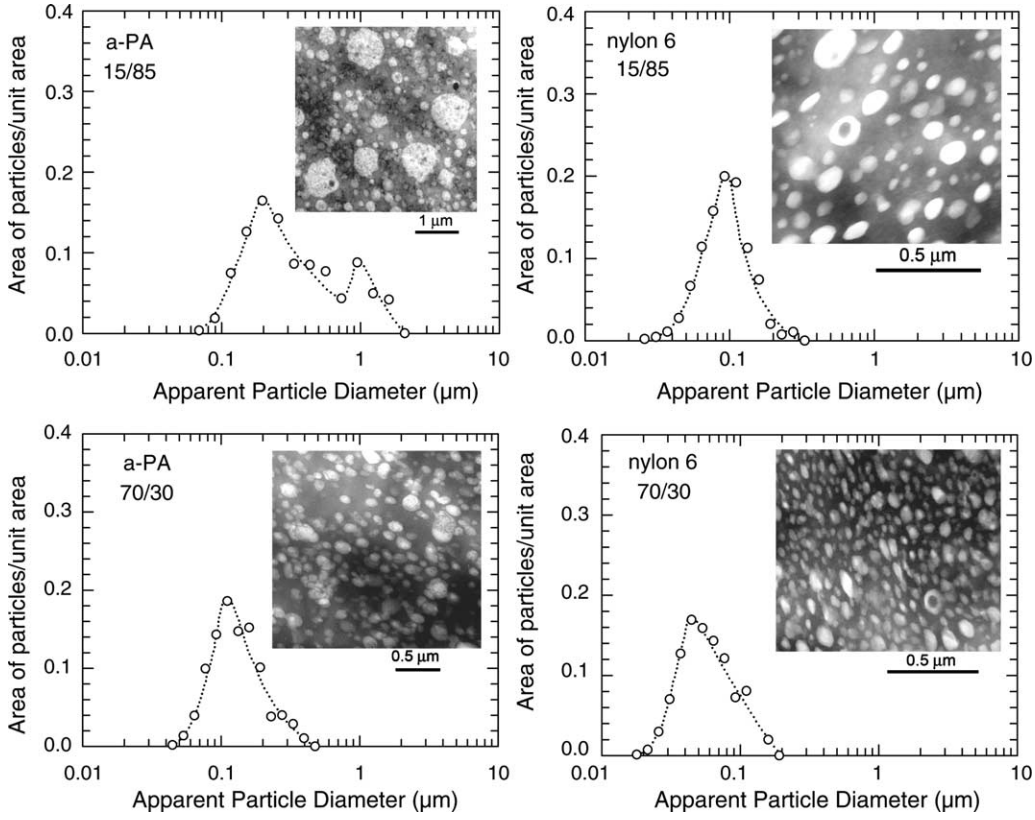

Fig. 10. TEM photomicrographs and rubber particle size distributions for ternary blends based on EOR-g-MA-2.5%/EOR-g-MA-0.35% in proportions of 15:85 and 70:30 when the total rubber phase is fixed at 20 wt% for each of the two matrices. The polyamide phase is stained dark with phosphotungstic acid.

Table 4
Rubber particle size comparison viewed perpendicular versus parallel to the flow direction (FD) for selected blends

Matrix	Rubber phase (20 wt%)	Examined direction	Modality	$\bar{d}_w$ (μm)[a]	$\bar{d}_w/\bar{d}_n$	$\bar{d}_v/\bar{d}_n$
a-PA	EOR-*g*-MA-2.5%/EOR = 16:84	⊥FD	Bimodal[a]	0.093	1.16	1.63
				0.98	1.16	1.41
		‖FD	Bimodal[a]	0.087	1.16	1.57
				1.71	1.41	1.93
Nylon 6	EOR-*g*-MA-1.6%/EOR = 28:72	⊥FD	Bimodal[a]	0.091	1.15	1.61
				0.51	1.18	1.73
		‖FD	Bimodal[a]	0.085	1.20	1.96
				0.63	1.13	1.38

[a] Particle size and distribution given for each population.

electrons in its annular dark field detectors [46]. The phase contrast can be enhanced even further by adjusting the signal-processing control and the contrast and brightness controls on the cathode-ray tube (CRT); these features are not available in traditional TEM. Furthermore, STEM is quite useful when the sections are thick and beam sensitive and when contrast is more important than resolution.

5.2.3. Effect of the ratio of elastomer components on morphology

Fig. 10 shows representative examples of how the ratio of the two elastomer components, in this case, the ratio of EOR-*g*-MA-2.5%/EOR-*g*-MA-0.35%, affects the morphology development of the blend. When their ratio is 15:85, a partially developed bimodal distribution of particle sizes is seen for the a-PA blend; however, unlike the case shown in Fig. 7 where the bimodality is observed for both polyamides where the ratio is 16:84, the nylon 6 blend shows a unimodal distribution of particle sizes. Bimodality in morphology sometimes can be seen directly from the TEM photomicrographs; however, quantification of the rubber particle size distribution is still necessary since the distribution is more objective and is particularly useful when the distribution seems to be in conflict with what one sees by eye in TEM images. Thus, the matrix as well as the ratio between the elastomers affects the morphology development, a unimodal distribution of particle sizes is observed for both matrices when the ratio is 70:30.

When the particles are not spherical, the direction of TEM viewing matters. Table 4 compares the rubber particle sizes examined in views parallel and perpendicular to flow direction for selected blends. As demonstrated by the examples shown by these two blends with bimodal distributions, only the larger particles show significant differences in size when examined parallel or perpendicular to the flow direction. For small rubber particles, these differences are very slight.

Fig. 11 shows the rubber particle polydispersity, expressed as the ratio of the volume to number average particle sizes, i.e. $\bar{d}_v/\bar{d}_n$, as a function of the proportions of the two elastomers. Here, unlike the cases shown in Tables 3–6, the global average particle sizes were used for the calculation of average particle size regardless of modality. For a-PA, the polydispersity shows a maximum at high EOR contents in its mixtures with EOR-*g*-MA-*X*% where $X = 1.6$ and 2.5. This maximum is associated with the emergence of bimodality. The polydispersity for blends containing EOR mixtures with EOR-*g*-MA-0.35% is relatively small across the spectrum of composition. Similarly, for nylon 6, a maximum in polydispersity is seen for blends containing mixtures of EOR with EOR-*g*-MA-*X*% where $X = 1.6$ and 2.5 in the region of high EOR content.

5.2.4. Effect of the order of mixing on morphology development

Fig. 12 shows the morphology and rubber particle size distribution for a ternary blend of nylon 6 containing EOR-*g*-

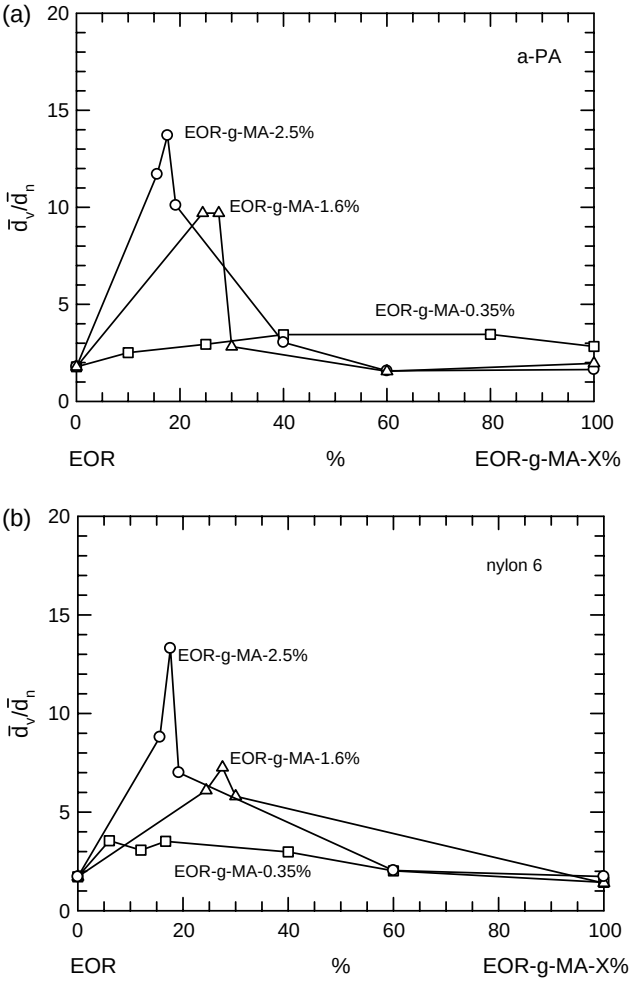

Fig. 11. Global polydispersity ratio, $\bar{d}_v/\bar{d}_n$, as a function of the ratio of EOR-*g*-MA-*X*% versus EOR in the rubber phase for ternary blends based on 20 wt% of EOR-*g*-MA-*X*%/EOR where the matrix is a-PA (a) and nylon 6 (b).

Table 5
Effect of the order of mixing on rubber particle size and distribution for selected blends of a-PA and blends of nylon 6

Matrix	Rubber phase (20%)	Extruder	Order of mixing	Modality	$\bar{d}_w$ (μm)	$\bar{d}_w/\bar{d}_n$	$\bar{d}_v/\bar{d}_n$
a-PA	EOR-*g*-MA-0.35%/EOR = 25:75	Twin	Simultaneous	Unimodal	0.75	1.59	2.94
			Premixed	Unimodal	0.78	1.90	2.39
	EOR-*g*-MA-0.35%/EOR = 80:20	Twin	Simultaneous	Unimodal	0.31	1.32	3.45
			Master batch	Unimodal	0.28	1.39	3.82
a-PA	EOR-*g*-MA-2.5%/EOR = 18:82	Twin	Simultaneous	Bimodal[a]	0.092	1.16	1.66
					1.06	1.21	1.50
		Twin	Premixed	Bimodal[a]	0.10	1.26	2.42
					1.18	1.32	1.85
	EOR-*g*-MA-2.5%/EOR = 60:40	Twin	Simultaneous	Unimodal	0.11	1.21	1.57
			Master batch	Unimodal	0.11	1.20	1.74
Nylon 6	EOR-*g*-MA-0.35%/EOR = 17:83	Twin	Simultaneous	Unimodal	0.38	1.65	3.52
			Master batch	Unimodal	0.40	1.39	2.11
	EOR-*g*-MA-0.35%/EOR = 60:40	Twin	Simultaneous	Unimodal	0.15	1.21	2.02
			Master batch	Unimodal	0.16	1.18	1.65
Nylon 6	EOR-*g*-MA-2.5%/EOR = 18:82	Twin	Simultaneous	Bimodal[a]	0.078	1.16	1.72
					0.71	1.28	1.99
		Twin	Master batch	Bimodal[a]	0.094	1.34	2.49
					0.57	1.07	1.23
	EOR-*g*-MA-2.5%/EOR = 60:40	Twin	Simultaneous	Unimodal	0.062	1.22	2.04
			Master batch	Unimodal	0.057	1.16	1.78

[a] Particle size and distribution given for each population.

MA-2.5% and EOR in a ratio of 18:82 where three different order of mixing protocols were used for melt compounding: simultaneous addition of all the components, premixing of the two components in the rubber phase first and then melt blending with nylon 6, and formation of a master batch of nylon 6 with the non-maleated EOR elastomer and then melt blending with additional nylon 6 and the maleated EOR material. Again, a bimodal particle size distribution appears regardless of the melt protocol. Thus, the order of mixing does not seem to influence the bimodality. Table 5 summarizes the effect of the order of mixing of the components on the average rubber particle size and the polydispersity for selected blends. The order of mixing of the components seems to cause negligible difference in the average size of the particles or their polydispersity for blends with a unimodal particle size distribution regardless of the matrix; however, for blends having a bimodal particle size distribution, the order of mixing seems to affect the rubber particle size a little more but still not significantly. The premixed approach in a-PA blend with a bimodal distribution seems to lead to a greater size for the larger particles, while the master batch in nylon 6 blend with a bimodal particle size distribution tends to lead to a smaller size for the larger particles than the case when all the components were added simultaneously.

5.2.5. *Effect of the extruder type on morphology development*

The previous research on ternary blends of a-PA with maleated and non-maleated SEBS has shown that twin screw extrusion generally yields blends with higher Izod impact strength and lower ductile–brittle transition temperatures than do blends of the same composition formed by single screw extrusion. Thus, only twin screw extrusion is used in this study in the formulation of blends containing a-PA. We have found that the intensity of mixing or extruder type affects the average particle size as might be expected; however, the choice of extruder does not seem to affect whether there is a bimodal particle size distribution or not. This conclusion applies to the particular equipment and materials used here and may not be

Table 6
Effect of the extruder type on rubber particle size and distribution for blends of nylon 6 based on EOR-*g*-MA-0.35%/EOR and EOR-*g*-MA-2.5%/EOR

Rubber phase (20%)	Extruder type	Order of mixing	Modality	$\bar{d}_w$ (μm)	$\bar{d}_w/\bar{d}_n$	$\bar{d}_v/\bar{d}_n$
EOR-*g*-MA-0.35%/EOR = 17:83	Twin	Simultaneous	Unimodal	0.38	1.65	3.52
	Single	Simultaneous	Unimodal	0.54	1.83	3.64
	Twin	Master batch	Unimodal	0.40	1.39	2.11
	Single	Master batch	Unimodal	0.58	1.97	4.63
EOR-*g*-MA-0.35%/EOR = 60:40	Twin	Master batch	Unimodal	0.16	1.18	1.65
	Single	Master batch	Unimodal	0.37	1.53	3.42
EOR-*g*-MA-2.5%/EOR = 18:82	Twin	Master batch	Bimodal[a]	0.094	1.34	2.49
				0.57	1.07	1.23
	Single	Master batch	Bimodal[a]	0.14	1.28	2.17
				1.06	1.21	1.60
EOR-*g*-MA-2.5%/EOR = 60:40	Twin	Master batch	Unimodal	0.057	1.16	1.78
	Single	Master bach	Unimodal	0.095	1.53	3.65

[a] Particle size and distribution given for each population.

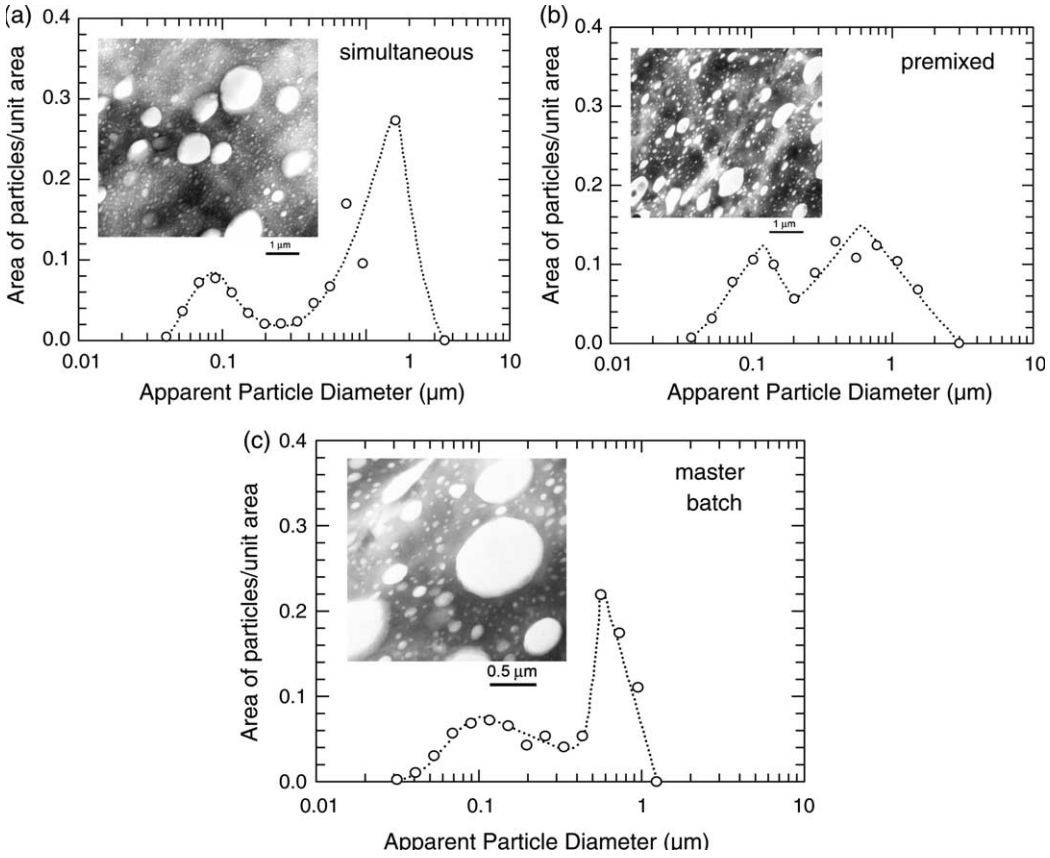

Fig. 12. Effect of the order of mixing of the components on morphology and rubber particle size distribution for a ternary blend of nylon 6 containing 20 wt% EOR-*g*-MA-2.5%/EOR in a proportion of 18:82 where the order of mixing of the components was simultaneous (a), premixing of the rubber phase (b), and formation of a master batch of nylon 6 with the non-maleated EOR material (c) as described in the text.

general for all other situations. Fig. 13 shows the rubber particle size distribution for the same blend of nylon 6 via a master batch where the rubber phase contains EOR-*g*-MA-2.5%/EOR in a proportion of 18:82 as shown in Fig. 12 but prepared in a single screw extruder. In both cases, a bimodal particle distribution is observed. The extruder type does not seem to affect the bimodality. Table 6 shows the effect of the extruder type on rubber particle size for selected blends of nylon 6. The blends prepared in the single screw extruder show larger sizes compared with those made in a twin screw extruder, as might be expected from the less intensive mixing of the single screw extruder.

5.2.6. Map of bimodal versus unimodal particle size distributions

The previous sub-sections described how the rubber phase maleic anhydride level, miscibility of the two elastomers, the proportions of the two elastomers, the order of mixing, and mixing intensity influenced morphology development in EOR-based blends with nylon 6 and a-PA. It is shown that the order of mixing and mixing intensity do not seem to affect, at least qualitatively, the modality of rubber particle morphology, although the two factors influence the size to some extent. However, it appears that the miscibility of the two elastomers and the proportions of the two EOR materials comprising the rubber phase in the nylon 6 and a-PA matrices are the main factors that affect whether bimodality occurs or not. It is useful to sort these out in a more logic way to demonstrate how each of them governs the modality in particle size distributions of blends. Fig. 14 shows a map for each matrix in which we show the results for many different blend systems. Each system is located by plotting the relative proportions of the more highly

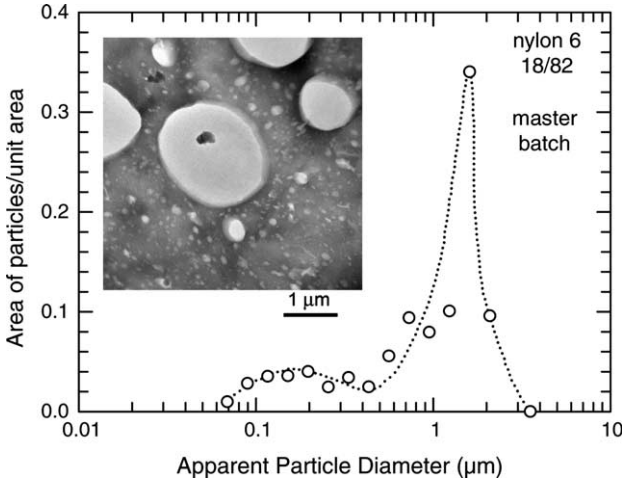

Fig. 13. Effect of the extruder type on the morphology and rubber particle size distribution for the ternary blend of nylon 6 shown in Fig. 12, but made by single screw extrusion, with a total 20 wt% content of EOR-*g*-MA-2.5%/EOR in a proportion of 18:82.

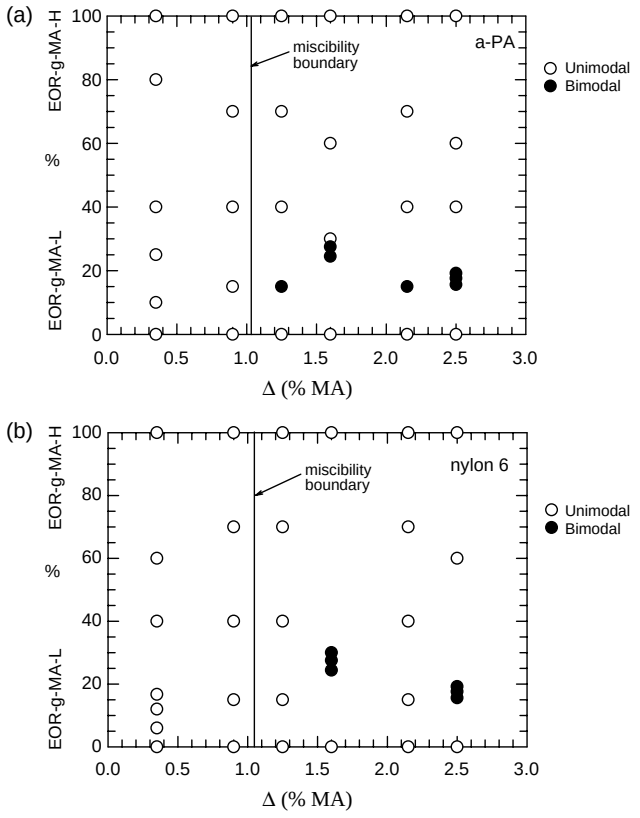

Fig. 14. Map of bimodal and unimodal particle size distributions for blends of a-PA (a) and blends of nylon 6 (b) containing total 20 wt% elastomers in which the relative proportion of the more highly, EOR-*g*-MA-H, and the less highly maleated EOR-*g*-MA-L, ethylene-1-octene copolymers in the rubber phase is plotted versus the difference in maleation level of the two EOR elastomers.

maleated, EOR-*g*-MA-H, and the less highly maltead, EOR-*g*-MA-L, ethylene-1-octene copolymers that comprise the rubber phase in 80:20 polyamide/rubber blends versus the difference in maleation level of the two EOR-based materials. The open points represent blends that showed a unimodal distribution of rubber particles and this did not seem to be affected by any other variable within the range investigated. The filled circles represent blends exhibiting bimodal distributions. When the Δ(%MA) was below the limit where the two elastomers were determined to be miscible, unimodal distributions were observed in all cases regardless of the matrix type or ratio of the two elastomer components. However, when the two elastomers exceed the critical Δ(%MA) for miscibility, bimodality tends to occur when the content of the more highly maleated EOR in the rubber phase is low while unimodality prevails when the content of EOR-*g*-MA-H is higher. Interestingly, for nylon 6, unlike the case of a-PA, a bimodal distribution of particle sizes is not observed even at a low content of EOR-*g*-MA-H when the rubber phase consists of the immiscible pairs EOR-*g*-MA-1.6%/EOR-*g*-MA-0.35% and EOR-*g*-MA-2.5%/EOR-*g*-MA-0.35%. The failure to observe bimodal distributions of particle sizes in these cases may be attributed to the fact that the sizes formed from each of the two elastomers alone with nylon 6 are too close to be resolved as can be seen in Fig. 3. In these cases, there is still likely to be two distinct groups of particles due to the immiscibility of the two elastomers; however, the two groups simply cannot be distinguished by their sizes.

6. Conclusions

The elastomer particle morphology in ternary blends of maleated and non-maleated ethylene-based elastomers with polyamides has been investigated. Two types of elastomers, EPR with its maleated version, EPR-*g*-MA, and EOR with its maleated versions, EOR-*g*-MA-*X*%, and two classes of polyamides, a-PA and nylon 6, have been employed in the formulation of the ternary blends. Morphology development of the ternary blends was examined in terms of both thermodynamic and kinetic factors. Both can influence the morphology development; the thermodynamic state of miscibility of the two types of elastomers always must be considered but some of the kinetic factors are not always important. For polyamide blends with EPR-*g*-MA/EPR mixtures, owing to the fact that EPR and EPR-*g*-MA are miscible, the particle morphology is well controlled via the level of maleation in the rubber phase. The two types of polyamides were found to exhibit quite analogous morphology, i.e. the rubber particle sizes are about the same at the same maleation level, in this case. However, the elastomer particle morphology of polyamide blends with EOR-*g*-MA/EOR mixtures was found to be much more complex. For both matrices, the average particle size strongly depends on the level of maleation in the rubber phase. In general, the rubber particle size in a-PA blends is larger than that in nylon 6 blends most likely because the chain ends for the a-PA material are predominately carboxyl groups rather than amine groups, i.e. $[COOH]/[NH_2]=4.5$ as shown in Table 1, which reduces the possible frequency of grafting. Using a special staining technique combined with transmission electron microscopy, it was shown that EOR elastomers with different levels of maleation are miscible when the difference in level of maleation is less than Δ(%MA)$=0.9$ to 1.25% but they are immiscible at higher differences. When the two elastomers are miscible, the rubber particle size distribution was always found to be unimodal, regardless of all other factors examined. This seems entirely reasonable owing to the thermodynamic driving force for the two elastomers to maintain a single phase but of varying maleic anhydride content and, hence, particle size as their ratio is varied. However, when the two elastomers are immiscible, the blends could either exhibit a bimodal or a unimodal particle size distribution depending on the ratio of the elastomers and the matrix type. Immiscibility of the two elastomers in the ternary blends would seem naturally to lead to a bimodal particle size distribution, i.e. a group of distinctly small particles mixed with a group of distinctly large rubber particles, since thermodynamically the two elastomers resist mixing with each other. However, when the ratio of the more highly maleated EOR elastomer in the rubber phase becomes higher, a unimodal particle size distribution may result from the following causes. First, the graft chains formed by reaction of the amine groups of the polyamide with the maleic

anhydride of the EOR-*g*-MA material can significantly increase the melt viscosity of the blend which in turn leads to higher shear stresses that tend to make the domain size of the non-maleated EOR elastomer smaller. If the two distributions overlap significantly, they may not be distinguishable. Second, the polyamide grafted EOR-*g*-MA phase may encapsulate the non-maleated EOR rubber due to the thermodynamic affinity between the two elastomers to create a core-shell type structure. There might be a limit on how much EOR the grafted EOR-*g*-MA phase can encapsulate; this would cause a breakdown of the core-shell type structure at high EOR-*g*-MA/EOR ratios and lead to bimodality. Interestingly, the order of mixing or the extruder type does not seem to change the modality of the particle size distribution.

Acknowledgements

The authors are indebted to Dr Jean-Roch Schauder of the European Technology Center, ExxonMobil for numerous valuable technical communications, and to Srivatsan Srinivas of the Baytown Technology and Engineering Complex, ExxonMobil Chemical Company for measuring the density and molecular weight for the four neat EOR elastomers. The authors are also grateful to Dr Ji-Ping Zhou of the Texas Materials Institute, the University of Texas at Austin for helping with the STEM setup. The authors thank Honeywell International Inc., E.I. DuPont Co., PolyOne Distribution, and ExxonMobil Chemical Co. for providing the materials employed in these studies.

References

[1] Epstein BN. US Patent 4, 174, 358 (to E.I Dupont); 1979.
[2] Borggreve RJM, Gaymans RJ, Schuijer J, Housz JFI. Polymer 1987;28:1489.
[3] Pecorini TJ, Manson JA, Hertzberg RW. Polym Prepr 1988;29:136.
[4] Wu S. J Appl Polym Sci 1988;35:549.
[5] Xanthos M. Polym Eng Sci 1988;28:1392.
[6] Bucknall CB, Heather PS, Lazzeri A. J Mater Sci 1989;24:2255.
[7] Gilmore DW, Modic MJ. Plast Eng 1989;45:51.
[8] Brummel M, Neuhausl E, Sova M, Houska M, Hoffmanova L, Petru K. Plast Rubber Proc Appl 1990;13:243.
[9] Cecere A, Greco R, Ragosta G, Scarinzi G, Taglialatela A. Polymer 1990;31:1239.
[10] Oshinski AJ, Keskkula H, Paul DR. Polymer 1992;33:268.
[11] Oshinski AJ, Keskkula H, Paul DR. Polymer 1992;33:284.
[12] Takeda Y, Keskkula H, Paul DR. Polymer 1992;33:3173.
[13] Dijkstra K, ter Laak J, Gaymans RJ. Polymer 1994;35:315.
[14] Majumdar B, Keskkula H, Paul DR. Polymer 1994;35:1386.
[15] Muratoglu OK, Argon AS, Cohen RE, Weinberg M. Polymer 1995;36:921.
[16] Oshinski AJ, Keskkula H, Paul DR. Polymer 1996;37:4909.
[17] Oshinski AJ, Keskkula H, Paul DR. Polymer 1996;37:4891.
[18] Oostenbrink AJ, Molenaar LJ, Gaymans RJ. PRI Conf Polym Blends, Cambridge 1990.
[19] Bucknall CB. Deformation mechanisms in rubber-toughened polymers. In: Paul DR, Bucknall CB, editors. Polymer blends. 2nd ed. New York: Wiley; 2000. p. 83.
[20] Gaymans RJ. Toughening semicrystalline thermoplastics. In: Paul DR, Bucknall CB, editors. Polymer blends. 2nd ed. New York: Wiley; 2000. p. 177.
[21] Borggreve RJM, Gaymans RJ, Eichenwald HM. Polymer 1989;30:78.
[22] Gaymans RJ, Borggreve RJM. Toughening mechanism in polyamide-rubber blends. In: Culbertson BM, editor. Contemporary topics in polymer science. New York: Plenum Press; 1989. p. 461.
[23] Dijkstra K, Gaymans RJ. Polymer 1993;34:3313.
[24] Dijkstra K, Van Der Wal A, Gaymans RJ. J Mater Sci 1994;29:3489.
[25] Janik H, Gaymans RJ, Dijkstra K. Polymer 1995;36:4203.
[26] Argon AS, Bartczak Z, Cohen RE, Muratoglu OK. Novel mechanisms of toughening semi-crystalline polymers. In: Pearson RA, Sue HJ, Yee AF, editors. Toughening of plastics: advances in modeling and experiments. ACS symposium series, vol. 759. Washington, DC: American Chemical Society; 2000. p. 98.
[27] Corte L, Beaume F, Leibler L. Polymer 2005;46:2748.
[28] Huang JJ, Keskkula H, Paul DR. Polymer 2004;45:4203.
[29] Yu Z-Z, Ke Y-C, Ou Y-C, Hu G-H. J Appl Polym Sci 2000;76:1285.
[30] Yu Z-Z, Ou Y-C, Hu G-H. J Appl Polym Sci 1998;69:1711.
[31] Gonzalez-Montiel A, Keskkula H, Paul DR. J Polym Sci, Part B: Polym Phys 1995;33:1751.
[32] Huang JJ, Keskkula H, Paul DR. Polymer, in press, doi: 10.1016/j.polymer.2005.11.088.
[33] Huang JJ, Keskkula H, Paul DR. Polymer. submitted for publication.
[34] Ellis TS. Macromolecules 1991;24:3845.
[35] Personal communications with Schauder JR; 2003.
[36] Corte L, Leibler L. Polymer 2005;46:6360.
[37] Trent JS, Scheinbeim JI, Couchman PR. Macromolecules 1983;16:589.
[38] Xanthos M, Parmer JF, La Forest ML, Smith GR. J Appl Polym Sci 1996;62:1167.
[39] Flory PJ. Principles of polymer chemistry. Ithaca, NY: Cornell University Press; 1953.
[40] Koningsveld R, Chermin HAG, Gordon M. Proc R Soc London, Ser A 1970;319:331.
[41] Koningsveld R, Kleintjens LA, Schoffeleers HM. Pure Appl Chem 1974;39:1.
[42] Koningsveld R, Kleintjens LA. J Polym Sci, Polym Symp 1977;61:221.
[43] Kambour RP, Bendler JT, Bopp RC. Macromolecules 1983;16:753.
[44] Ten Brinke G, Karasz FE, MacKnight WJ. Macromolecules 1983;16:1827.
[45] Paul DR, Barlow JW. Polymer 1984;25:487.
[46] Williams DB, Carter CB. Transmission electron microscopy: a textbook for materials science. New York: Plenum Press; 1996.